applied sciences

MDPI

Article

Numerical Analysis of Newtonian Heating Convective Flow by Way of Two Different Surfaces

Khalil Ur Rehman [1,2,*], Wasfi Shatanawi [1,3,*], Shazia Ashraf [2] and Nabeela Kousar [2]

1 Department of Mathematics and Sciences, College of Humanities and Sciences, Prince Sultan University, Riyadh 11586, Saudi Arabia
2 Department of Mathematics, Air University, PAF Complex E-9, Islamabad 44000, Pakistan; 191757@students.au.edu.pk (S.A.); nabeela@mail.au.edu.pk (N.K.)
3 Department of Mathematics, Faculty of Science, The Hashemite University, P.O. Box 330127, Zarqa 13133, Jordan
* Correspondence: kurrehman@psu.edu.sa (K.U.R.); wshatanawi@psu.edu.sa (W.S.)

Abstract: In this paper, we offer a numerical study on heated non-Newtonian fluid with a Newtonian heating effect towards thermally stable stretching surfaces. A comparative analysis for two stretched surfaces, namely, plate and cylinder, is offered. The Casson fluid model is considered to be a non-Newtonian fluid model. By applying the suitable set of transformations, the non-linear coupled PDEs are transformed into non-linear ODEs. It is difficult to obtain the exact solution of such non-linear differential equations; therefore, we used the shooting method along with Runge–Kutta scheme. The influence of pertinent flow variables on velocity and temperature is presented through graphs. Notably from the results, heat generation parameters, Newtonian heating, and magnetic parameters enhanced the temperature profile, whereas Casson fluid and magnetic field parameters reduced the fluid velocity. It is also observed that increases in fluid temperature were more influenced at the cylindrical surface as compared with the flat plate. Moreover, we obtained remarkable results for the heat transfer rate by imposing Newtonian heating conditions at the surface; tables are used to present variations in the skin friction coefficient and Nusselt number at the thermally stable surfaces.

Keywords: Newtonian heating; heat sink/source; cylindrical/flat surface; shooting method; MHD

Citation: Rehman, K.U.; Shatanawi, W.; Ashraf, S.; Kousar, N. Numerical Analysis of Newtonian Heating Convective Flow by Way of Two Different Surfaces. *Appl. Sci.* **2022**, *12*, 2383. https://doi.org/10.3390/app12052383

Academic Editor: Hijaz Ahmad

Received: 26 December 2021
Accepted: 22 February 2022
Published: 24 February 2022

1. Introduction

Analysis of heat transfer phenomena in fluid mechanics has showed that it has a vital role in many engineering and technological processes, such as glass fiber manufacturing, plastic sheeting, and food processing, to name a few. Heat transfer mechanisms have applicable uses in our daily life, through conduction, convection, and radiation. Particularly, heat transfer analysis in Newtonian and non-Newtonian fluid models has gained great interest from many researchers in recent years, due to their wide range of applications in industry. Mostly, scientists have focused on the study of the boundary layer flow of both fluid models and the heat transfer analysis by including linear, nonlinear, exponential, hyperbolic, and cylindrical stretching surfaces; Crane [1], for instance, introduced the concept of a boundary layer towards stretching sheet taking with linear velocity. He also obtained an exact solution for the flow equation in this problem. Gupta and Gupta [2] presented a heat transfer study along with mass transfer aspects subject to stretching sheets, having applications in polymer processing. The temperature distribution in a viscous incompressible fluid flow induced by the stretching of a sheet that emerges through a slit into the stream was investigated by Dutta et al. [3]. The sheet velocity was proportional to its distance from the slit, and it was subjected to a constant heat flux. It was discovered that when the Prandtl number rises, the temperature at a given location falls. The temperature of the stretched sheet is calculated for multiple Prandtl numbers for a given surface heat flow. The heat transfer happening in the laminar boundary layer on a linearly stretched, continuous surface subjected to suction or blowing was investigated by Char [4]. Two scenarios were considered: a sheet with a predetermined wall temperature, and a sheet with a predetermined heat flux. Kummer's functions were used to express the findings. The answers were reduced to the reported findings under certain circumstances. Additionally, the findings of an impermeable stretched plate with varying wall heat flux were acquired. Finally, the impacts of the Prandtl number, the suction or blowing parameter, the temperature parameter, and the heat flux parameter on the temperature distribution were thoroughly studied. The flow and heat transfer properties of a viscous fluid across a nonlinearly extending sheet were investigated by Vajravalu [5]. The flow and heat transfer equations of the conservation of momentum, mass, and energy were partially decoupled using a similarity transformation that was distinct from the linearly stretched sheet issue. Using a fourth-order Runge–Kutta integration strategy, the fundamental nonlinear differential equation for the velocity field and the differential equation with a variable coefficient for the temperature field were numerically solved. A table and graphs were used to display the numerical data for the flow and heat transfer characteristics. Furthermore, it was demonstrated that heat flowed from the stretched sheet to the fluid at all times. Radiation influences on the boundary layer flow and heat transfer of a viscous fluid across an exponentially stretched sheet were investigated by Sajid and Hayat [6]. The convergent series expressions of velocity and temperature were determined using the homotopy analysis method (HAM). Graphs were used to lend a physical explanation to these expressions. The effects of Prandtl and radiation numbers on temperature were discovered to be diametrically opposed. The problem of laminar fluid flow in a nanofluid caused by the stretching of a flat surface was quantitatively studied by Khan and Pop [7]. This is the first paper on nanofluid stretching sheets. The Brownian motion and thermophoresis effects are accounted for in the nanofluid model. The Prandtl number, Lewis number, Brownian motion number, and thermophoresis number all play a role in the similarity solution. Tables and graphs were used to show the variance in the reduced Nusselt and reduced Sherwood values. The reduced Nusselt number was discovered to be a decreasing function of each dimensionless number, but the reduced Sherwood number was found to be an increasing function of the higher Prandtl number. In addition, heat transfer in non-Newtonian fluids is also acknowledged by researchers, such as the boundary layer flow of Sisko fluid across a stretched cylinder, which was investigated by Malik et al. [8]. In heat transmission, the combined effects of variable thermal conductivity and viscous dissipation were postulated. Using appropriate transformations, the modeled boundary layer partial differential equations were transformed into ordinary differential equations. The Runge–Kutta–Fehlberg technique was used to numerically solve these nonlinear ordinary differential equations. By comparing the computed findings with those in the available literature, the correctness of the results was confirmed. Graphs were created to analyze the impact of flow parameters on velocity and temperature profiles. The impact of all physical factors on the skin friction coefficient and local Nusselt number was examined in tabular and graphical form. The numerical solution of mixed convection tangent hyperbolic fluid flow towards stretched cylindrical surface with heat transfer issues was the focus of Rehman et al. [9]. The fluid flow was achieved by ensuring that there was no slippage. Partial differential equations were used to simulate the flow regime features. Partial differential equations were transformed into linked non-linear ordinary differential equations via a similarity transformation. To forecast numerical results, a computer approach was used. The effects of flow control factors such as mixed convection, thermal stratification, and solutal stratification on velocity, temperature, and concentration were investigated and the graphical results are shown. The influence of non-linear surface radiation on Casson-dusty particle suspension flow across a vertical wavy cone was investigated by Siddiqa et al. [10] as a heat transfer boundary layer analysis. To represent the contribution of surface radiative heat flow, the Stefan–Boltzmann law was used in the boundary conditions. To change the governing equations into non-dimensional, non-conserved form, appropriate sets of transformations were utilized; then, a numerical approach was used to acquire the solutions. The numerical findings were shown visually as a function of non-dimensional parameters. The results were compared with those found in the literature, and they were found to be in good agreement. The effects of non-linear radiation on heat transmission in MHD Casson nanofluid along a thin needle were examined by Souayeh et al. [11]. The issue was theoretically simulated, with the thermo-diffuso and diffuso-thermo effects taken into consideration. There were two sorts of surfaces treated here: fixed needle and moving needle. Using similarity variables, the Prandtl boundary layer equations were encapsulated and numerically solved. The effects of various material properties on momentum, temperature, and species concentration, as well as values relating to engineering considerations such as the skin friction coefficient, rate of energy transfer, and Sherwood number, were calculated and graphed. We assessed recent attempts on heat transfer development in Newtonian and non-Newtonian fluid models with various physical effects in [12–30].

Notably, individual studies on flat and cylindrical surfaces are reported on Casson fluid flow with various physical effects, and it seems difficult to conclude the comparison because of different solution techniques and assumptions. Therefore, in this study, we offer a comparative analysis of Casson fluid flow over both plate and cylindrical surfaces with the presence of a Newtonian heating effect. More specifically, we consider a simultaneous magnetized convective flow of Casson fluid over the two different heated stretching surfaces. The Runge–Kutta scheme with a shooting approach was used to solve the altered governing equations numerically. The computations were performed using MATLAB software. Furthermore, graphs were also used to illustrate the impact of emerging parameters on velocity and fluid temperature. Moreover, the numerical results are displayed in tabular form of heat transfer rate and skin friction for plate and cylindrical surfaces. One can extend the idea to study the numerous non-Newtonian fluid models having engineering standpoints.

2. Mathematical Formulation

We considered the two-dimensional convective flow of non-Newtonian fluid past a stretching cylinder. The Casson fluid model is taken in this case as a non-Newtonian fluid. The magnetic field B_0 is induced along the radial direction of the cylinder. Moreover, the Newtonian heating condition is also imposed at the surface. We assumed that the temperature at the cylindrical surface was higher than the temperature outside the surface (i.e., ambient temperature), where $\overline{T} > \overline{T}_\infty$. The geometry of problem is given in Figure 1. For viscous cases, the basic conservation equations, continuity, momentum, and thermal energy are taken as.

$$\text{div } \overline{\mathbf{V}} = 0, \tag{1}$$

$$\rho \frac{D\overline{\mathbf{V}}}{D\overline{t}} = \vec{\nabla}.\overline{\mathbf{T}} + \mu \vec{\nabla}^2 \overline{\mathbf{V}} + \overline{\mathbf{J}} \times \mathbf{B}, \tag{2}$$

$$\rho c_p \frac{d\overline{T}}{d\overline{t}} = K_1 \overline{\nabla}^2 \overline{T}. \tag{3}$$

With the following assumptions:

- For axisymmetric flow, there is no tangential velocity $(\overline{u}_\theta = 0)$;
- Taking velocity field as $\overline{\mathbf{V}} = [\overline{v}(\overline{x}, \overline{r}),\ 0, \overline{u}(\overline{x}, \overline{r})]$;
- Approximation of the boundary layer is incorporated here; accordingly, the pressure gradient is zero along the flow $p = p_0$, and variation in velocity along the radial direction is much smaller than in the axial direction, and the scale analysis for momentum equation with boundary layer theory is defined as: $\overline{u} \gg \overline{v},\ \frac{\partial \overline{u}}{\partial \overline{r}} >> \frac{\partial \overline{u}}{\partial \overline{x}}, \frac{\partial \overline{v}}{\partial \overline{x}}, \frac{\partial \overline{v}}{\partial \overline{r}} \Rightarrow \frac{\partial p}{\partial r} = 0$.

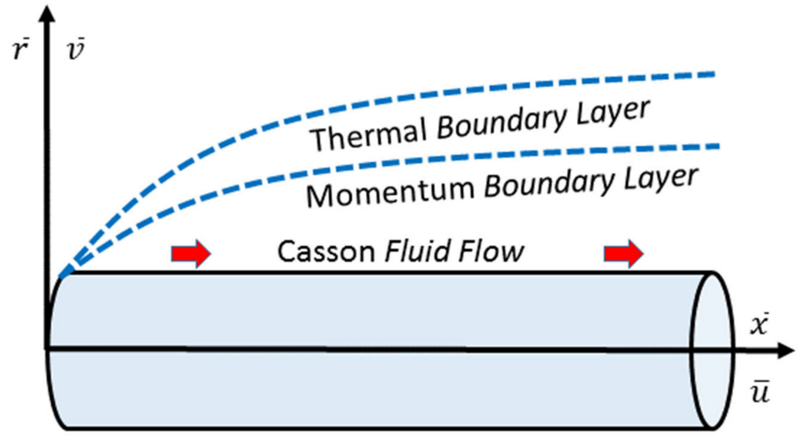

Figure 1. Geometry of the problem.

By using all the above assumptions and approximation, Equations (1)–(3), with the assumption of Casson fluid, can be reduced to the following component form:

$$\frac{\partial(\overline{r}\,\overline{u})}{\partial\overline{x}} + \frac{\partial(\overline{r}\,\overline{v})}{\partial\overline{r}} = 0, \tag{4}$$

$$\overline{u}\frac{\partial\overline{u}}{\partial\overline{x}} + \overline{v}\frac{\partial\overline{u}}{\partial\overline{r}} = v\left(1+\frac{1}{\beta}\right)\left(\frac{\partial^2\overline{u}}{\partial\overline{r}^2} + \frac{1}{\overline{r}}\frac{\partial\overline{u}}{\partial\overline{r}}\right) - \sigma\frac{B_0{}^2}{\rho}\overline{u} + g\beta^*{}_T(\overline{T} - \overline{T}_\infty), \tag{5}$$

$$\overline{u}\frac{\partial\overline{T}}{\partial\overline{x}} + \overline{v}\frac{\partial\overline{T}}{\partial\overline{r}} = \frac{K_1}{\rho c_p}\left(\frac{\partial^2\overline{T}}{\partial\overline{r}^2} + \frac{1}{\overline{r}}\frac{\partial\overline{T}}{\partial\overline{r}}\right) + \frac{Q_0}{\rho c_p}(\overline{T} - \overline{T}_\infty). \tag{6}$$

Here, $\overline{u}$ is the $\overline{x}$component of velocity and $\overline{v}$ is the $\overline{r}$components of velocity taken along axial direction and radial direction, respectively, v denotes the kinematic viscosity, σ indicates electric conductivity, and ρ is the fluid density. B_0 represents the magnetic field constant, g is used for the gravitational acceleration, Q_0 represents the heat generation/absorption coefficient, and $\beta^*{}_T$ indicates the thermal expansion coefficient. $\beta, \overline{T}, \overline{T}_\infty$ represent the Casson fluid parameter, surface temperature, and ambient temperature, respectively.

The BCs for the considered model are:

$$\begin{gathered}\overline{u} = \overline{u}_w = \tfrac{U_0\overline{x}}{L},\ \overline{v} = 0,\ \tfrac{\partial\overline{T}}{\partial\overline{r}} = -h_s\overline{T},\ \text{at}\ \overline{r} = \overline{R}, \\ \overline{u} \to 0, \overline{T} \to \infty,\ \text{as}\ \overline{r} \to \infty,\end{gathered} \tag{7}$$

where $\overline{u}(\overline{x}) = \frac{U_0\overline{x}}{L}$ is the linear velocity of the stretching cylinder, U_0 denotes the reference velocity, L is referred to as the characteristic length, h_s indicates the heat transfer coefficient, and $\overline{R}$ represents the radius of the cylinder.

The relationship of the stream function $\overline{\psi}$ with the velocity components is defined as:

$$\overline{u} = \frac{1}{\overline{r}}\frac{\partial\overline{\psi}}{\partial\overline{r}},\ \overline{v} = -\frac{1}{\overline{r}}\frac{\partial\overline{\psi}}{\partial\overline{x}}, \tag{8}$$

Now, to transform governing Equations (4)–(6) into nonlinear ODEs, we introduced suitable set of transformations [31], defined as:

$$\begin{gathered}\overline{u}(\overline{x}) = \tfrac{U_0\overline{x}}{L}f'(\eta),\ \overline{v} = -\tfrac{\overline{R}}{\overline{r}}\sqrt{\tfrac{U_0 v}{L}}f(\eta), \\ \eta = \tfrac{\overline{r}^2 - \overline{R}^2}{2\overline{R}}\left(\tfrac{U_0}{vL}\right)^{\frac{1}{2}},\ \theta(\eta) = \tfrac{\overline{T} - \overline{T}_\infty}{\overline{T}_\infty},\end{gathered} \tag{9}$$

where $f(\eta)$ and $\theta(\eta)$ represent the dimensionless velocity and temperature, respectively.

Thus, the continuity Equation (4) is satisfied identically. By inserting Equation (9) into Equations (5) and (6), we obtained:

$$ff'' - (f')^2 + \left(1 + \frac{1}{\beta}\right)[(1 + 2K\eta)f''' + 2Kf''] + \lambda\theta - \gamma^2 f' = 0, \tag{10}$$

$$(1 + 2K\eta)\theta'' + 2K\theta' + \Pr(f\theta' + Hp\theta) = 0. \tag{11}$$

Boundary conditions are transformed as:

$$f(0) = 0,\ f\prime(0) = 1,\ \theta'(0) = -\gamma_1[1 + \theta(0)]\,, \tag{12}$$

$$f'(\infty) \to 0,\ \theta(\infty) \to 0. \tag{13}$$

Here, $K, \lambda, \Pr, \gamma, Gr, \gamma_1$, and Hp denote the curvature parameter, mixed convection parameter, Prandtl number, magnetic field parameter, Grashof number, Newtonian heating parameter, and heat generation/absorption parameters, respectively. The mathematical relations for such involved parameters are:

$$\begin{gathered} K = \frac{1}{R}\sqrt{\frac{vL}{U_0}},\ \lambda = \frac{Gr}{\mathrm{Re}^2{}_x},\ \Pr = \frac{vc_p}{K_1}, \gamma = \sqrt{\frac{\sigma B^2{}_0 L}{\rho U_0}}, \\ G_r = \frac{g\beta^*{}_T \overline{T}_\infty x^3}{v^2}, \gamma_1 = \ h_s(\sqrt{\frac{vL}{U_0}}),\ Hp = \frac{LQ_0}{U_0\rho c_p}, \end{gathered} \tag{14}$$

Skin friction is the physical quantity that occurs when a fluid exerts a friction drag on a surface; this drag force is referred to as skin friction. It is described as:

$$\hat{C}_f = \frac{2\tau_w}{\rho U^2}, \tag{15}$$

where $\hat{C}_f$ is the skin friction and τ_w is the shear stress, which is directly proportional to the velocity gradient at the surface ($\overline{r} = \overline{R}$). It is defined as:

$$\tau_w = \mu\left(1 + \frac{1}{\beta}\right)\left(\frac{\partial\overline{u}}{\partial\overline{r}}\right)_{\overline{r}=\overline{R}}. \tag{16}$$

A physical quantity that calculates the rate of heat transfer at the surface is defined as:

$$\hat{N}u_x = \frac{xq_w}{K_1(\overline{T} - \overline{T}_\infty)}, \tag{17}$$

where $\hat{N}u_x$ denotes Nusselt number, q_w heat flux at the surface, which is proportional to temperature gradient at surface ($\overline{r} = \overline{R}$). It is expressed as follows:

$$q_w = -K_1\left(\frac{\partial\overline{T}}{\partial\overline{r}}\right)_{\overline{r}=R}. \tag{18}$$

By use of transformations, the dimensionless form of these quantities are:

$$\frac{1}{2}\hat{C}_f{\mathrm{Re}_x}^{1/2} = (1 + \frac{1}{\beta})f''(0), \tag{19}$$

$$\hat{N}u_x{\mathrm{Re}_x}^{-1/2} = -\theta'(0). \tag{20}$$

3. Numerical Scheme

The reduced equations for the fluid flow over the stretching cylinder are non-linear and highly coupled in nature. An analytical solution of these equations is difficult to find. To derive an approximate solution to the problem, a numerical technique is used: the shooting method with the Runge–Kutta fourth-fifth algorithm. For implementation of shooting method, one should convert the boundary value problem into the initial value problem. The reduce initial value problem is further converted into a system of first-order differential equations and then solved by choosing missing conditions as an initial guess. Therefore, the suitable transformations are used to obtained initial value problem. Here, the first-order differential system is obtained by the following procedure:

$$\begin{aligned}&f = m_1, \frac{df}{d\eta} = f' = m'_1 = m_2, \frac{d^2 f}{d\eta^2} = f'' = m_2{}' = m_3, \\ &\frac{d^3 f}{d\eta^3} = f''' = m_3{}', \theta = m_4, \frac{d\theta}{d\eta} = \theta' = m_4{}' = m_5.\end{aligned} \tag{21}$$

After putting the set of Equation (21) into Equations (10)–(13), we have:

$$\begin{aligned}&\frac{dm_1}{d\eta} = m_1{}' = m_2, \\ &\frac{dm_2}{d\eta} = m_2{}' = m_3, \\ &\frac{dm_3}{d\eta} = m_3{}' = \frac{(m_2)^2 - m_1 m_3 - (1+\frac{1}{\beta})2Km_3 - \lambda m_4 + \gamma^2 m_2}{(1+\frac{1}{\beta})(1+2K\eta)}, \\ &\frac{dm_4}{d\eta} = m_4{}' = m_5, \\ &\frac{dm_5}{d\eta} = m_5{}' = \frac{-2Km_5 - \Pr(m_1 m_5 + Hpm_4)}{(1+2K\eta)}.\end{aligned} \tag{22}$$

The corresponding BCs as follows:

$$\begin{aligned}&m_1(0) = 0, \\ &m_2(0) = 1, \\ &m_3(0) = U_1 \\ &m_4(0) = \theta(0) = U_2 \\ &m_5(0) = -\gamma_1(U_2 + 1).\end{aligned} \tag{23}$$

To solve the above system of Equation (22), the values of U_1 and U_2 are unknown; therefore, by taking a suitable initial guess, the convergent numerical solution is obtained. It is important to note that if the boundary residuals are less than the tolerance error 10^{-6}, the calculated solution converges. If the computed results do not satisfy this requirement, the initial estimates are changed using Newton's technique, and the procedure is repeated until the solution fulfills the specified convergence threshold.

4. Results and Discussion

In this study, Casson fluid, as a non-Newtonian fluid model, is considered simultaneously over stretched flat and cylindrical surfaces. The mixed convection, magnetic field, heat generation, heat absorption, and Newtonian heating are the physical effects assessed in this analysis. The mathematical modeling resulted with the following physical parameters: the Casson fluid parameter β, curvature parameter K, mixed convection parameter λ, magnetic parameter γ, Newtonian heating parameter γ_1, and heat generation/absorption parameter Hp. The numerical observations are concluded in terms of line graphs.

These figures have been plotted to examine the Casson fluid flow over a plate (zero curvature) and cylindrical surface (non-zero curvature). Mathematically, K = 0 denotes the flat surface, and K = 0.5 denotes the cylindrical surface. Figure 2 indicates the impact of the Casson fluid parameter β on the velocity profile $f'(\eta)$ over a stretched cylindrical surface. It is observed that the increments in parameter $\beta = 0.1, 0.3$ and 0.7 cause declines in fluid velocity. By physically increasing the Casson fluid parameter, the viscosity of fluid increases, and as a result, the fluid becomes more viscous, and consequently, the velocity reduces significantly.

The impact of parameter K on velocity $f'(\eta)$ over a cylindrical surface is depicted in Figure 3. It is evident from the figure that increments in parameter K = 0.1, 0.3 and 0.7 lead to an increase in fluid velocity, and an increase in the thickness of the boundary layer is also observed. Here, higher values in the curvature parameter reduce the radius of curvature; hence, Casson fluid particles have less interaction with the stretched surface. Such reduced interactions will offer less resistance to fluid particles, and as a result, the velocity shows a higher magnitude.

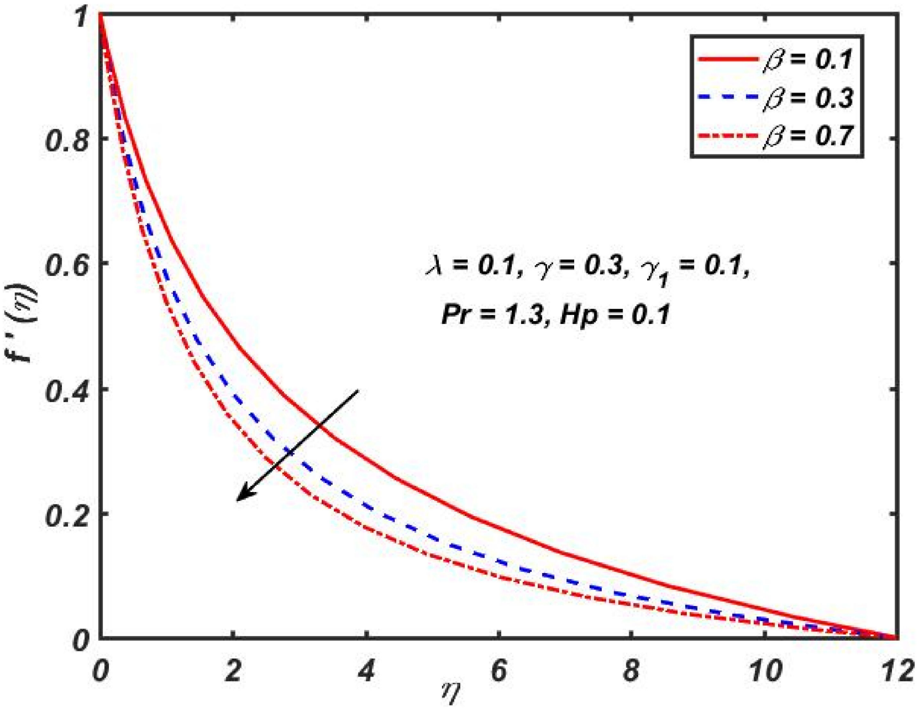

Figure 2. Effect of β on $f'(\eta)$.

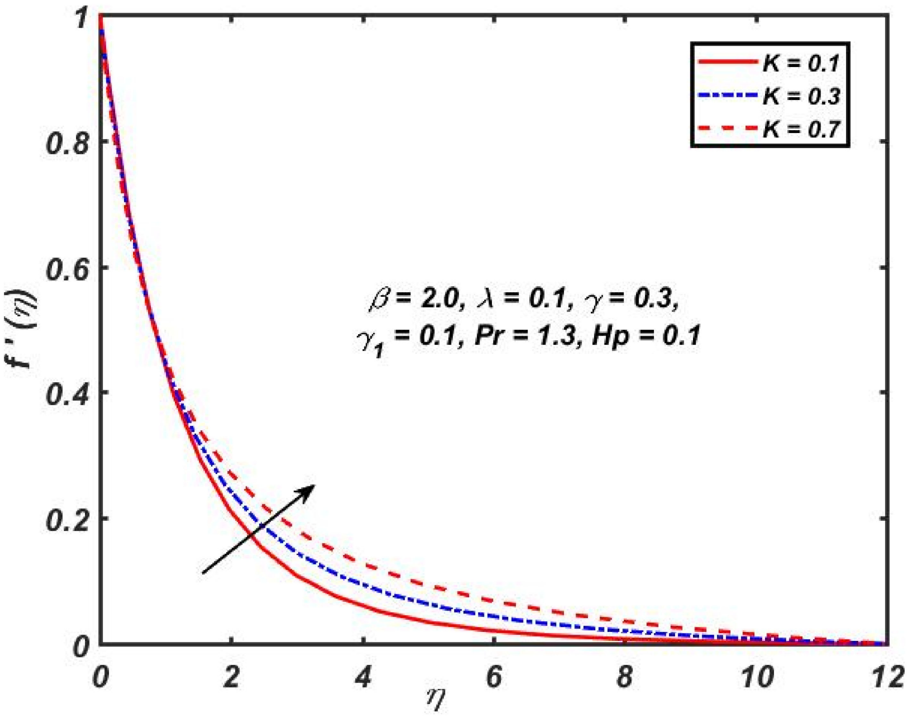

Figure 3. Effect of K on $f'(\eta)$.

Figure 4 shows that the rising value of the magnetic field parameter $\gamma = 0.1, 0.5$ and 0.9 causes a reduction in the magnitude of fluid velocity $f'(\eta)$, for both the stretched plate and cylindrical cases. This is due to the resistive force, named Lorentz force, which is enhanced when the magnetic field parameter is increased. This force offers resistance to the fluid flow, and consequently, velocity reduces. It is also observed that for the flow field over a cylindrical surface, the velocity magnitude is higher in strength as compared with the velocity of fluid over a flat surface. Figures 5–11 illustrate the effects of physical parameters on temperature $\theta(\eta)$. Figure 5 reveals that fluid temperature $\theta(\eta)$ rises for increments in curvature parameter K = 0.1, 0.3 and 0.7. This is because we noticed that for higher values of curvature parameter, the contact surface area reduces, and the resistance offered by the cylindrical surface reduces. This leads to an increase in the velocity of particles. The kinetic energy has a direct impact on the higher velocity. The higher velocity corresponds to a larger kinetic energy. The large value of average velocity results in higher temperature.

The impacts of Prandtl numbers Pr = 1.2, 1.4 and 1.6 on the temperature profile for the plate and cylinder is presented in Figure 6. It is evident from the figure that variation in the Prandtl number causes a reduction in fluid temperature $\theta(\eta)$, and a decline in the thermal boundary layer thickness is also observed for both the plate and cylinder. Here, the higher value of the Prandtl number causes a reduction in the thermal conductivity of fluid, and hence, the temperature profile for both the cylindrical and flat surface reduces significantly. It is observed from Figure 7 that increments in values of the parameter γ = 0.1, 0.7 and 1.0 render an increase in temperature $\theta(\eta)$. When the magnetic field increases, the Lorentz force increases. The resistance offered by the magnetic field causes particles to produce heat energy as a result, and the temperature for fluid flow over a flat and cylindrical surface increases. The impact of the Newtonian heating parameter γ_1 on temperature profile is illustrated in Figure 8 for both flat and cylindrical surfaces. We observed that the Newtonian heating parameter has a direct impact on the temperature profile. Furthermore, it is seen that the magnitude of the temperature profile is higher for cylindrical surfaces as compared with a flat plate for increasing values of the parameter γ_1. Newtonian heating enhances the fluid temperature for both surfaces.

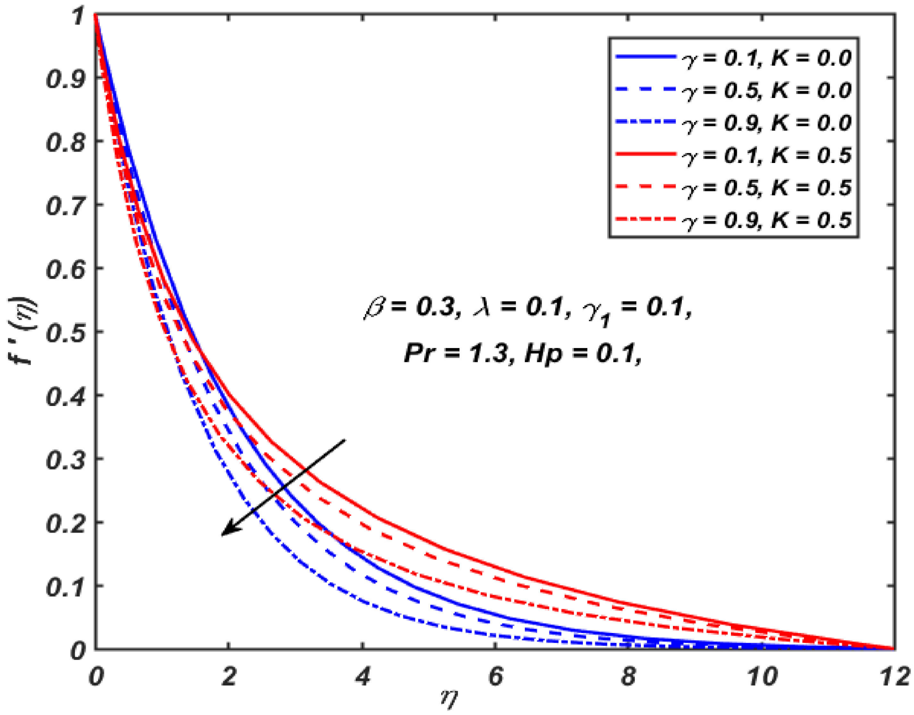

Figure 4. Effect of γ on $f'(\eta)$ for plate/cylinder.

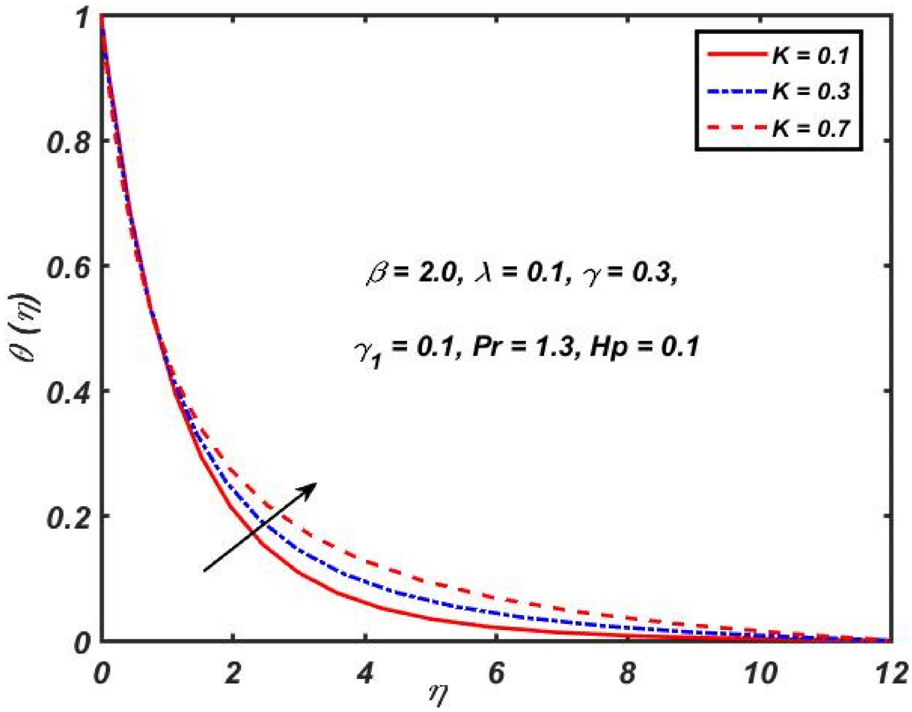

Figure 5. Effect of K on $\theta(\eta)$.

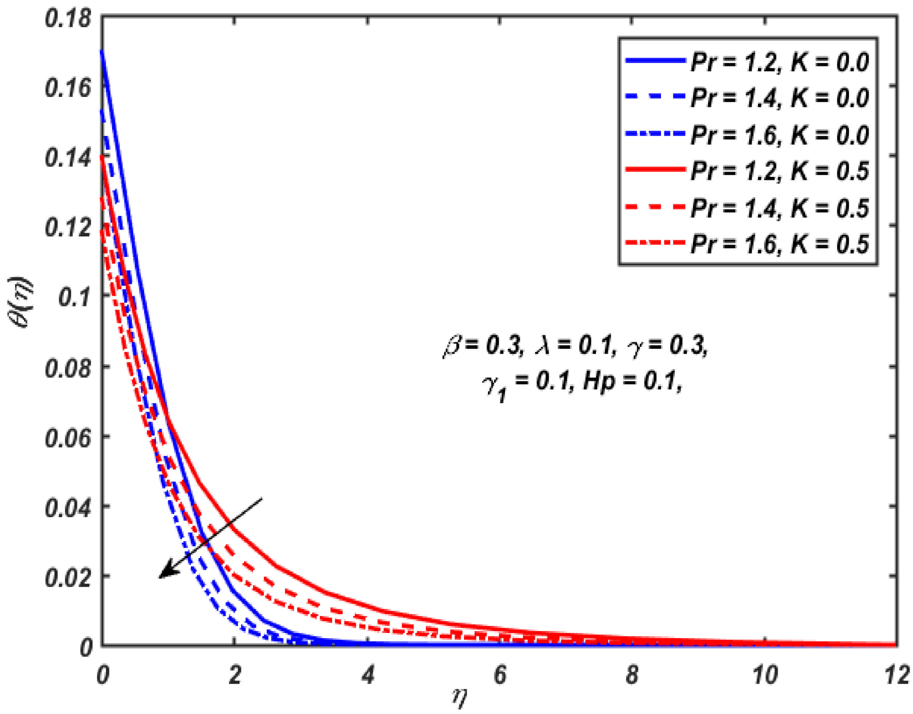

Figure 6. Effect of Pr on $\theta(\eta)$ for plate/cylinder.

Figures 9 and 10 demonstrate the impact of Hp^{+} = 0.1, 0.2, 0.3 (heat generation) parameter and Hp^{-} = −0.1, −0.2, −0.3 (heat absorption) parameter on temperature profile for both cylindrical and flat plate cases. From Figure 9, we observed that higher values of heat generation parameters produce heat energy, and as a result, the temperature of the fluid enhances. Such a trend is similar in the case of the flat and cylindrical surfaces. Figure 10 depicts the impact of heat absorption parameters on fluid temperature. We noticed that the temperature of Casson fluid over a flat and cylindrical surface decreases the function of the heat absorption parameter. This is because higher values of heat absorption parameters cause low heat energy and as a results temperature drops.

Figure 11 represents the impact of variations in the Casson fluid parameter β = 0.1, 0.3, 0.7 on temperature profile; with an increase in parameter β, the temperature of fluid over a cylinder increases.

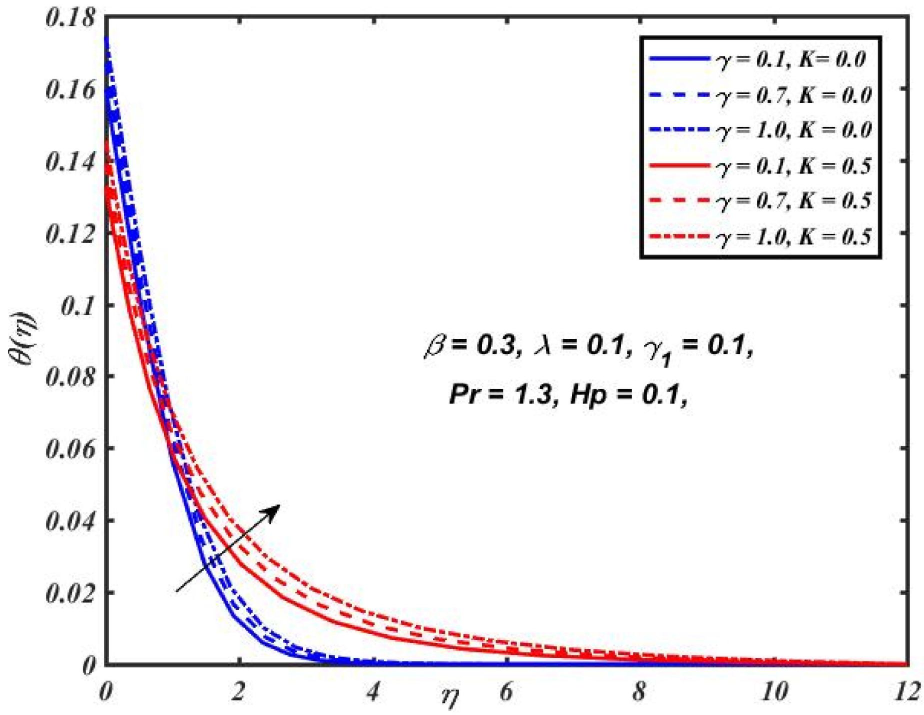

Figure 7. Effect of γ on $\theta(\eta)$ for plate/cylinder.

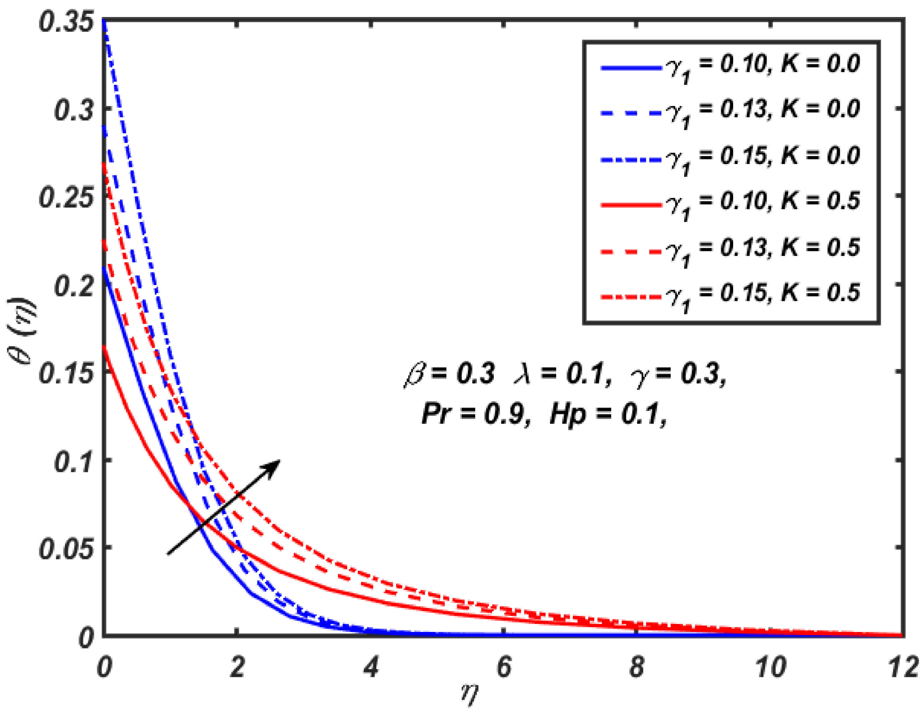

Figure 8. Effect of γ_1 on $\theta(\eta)$ for plate/cylinder.

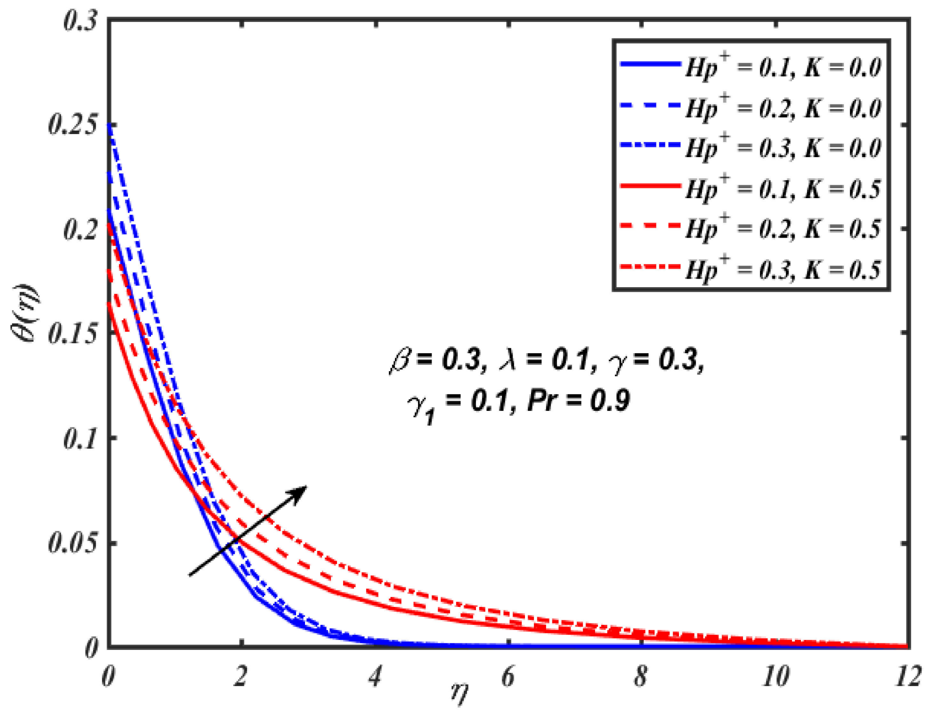

Figure 9. Effect of Hp^+ on $\theta(\eta)$ for plate/cylinder.

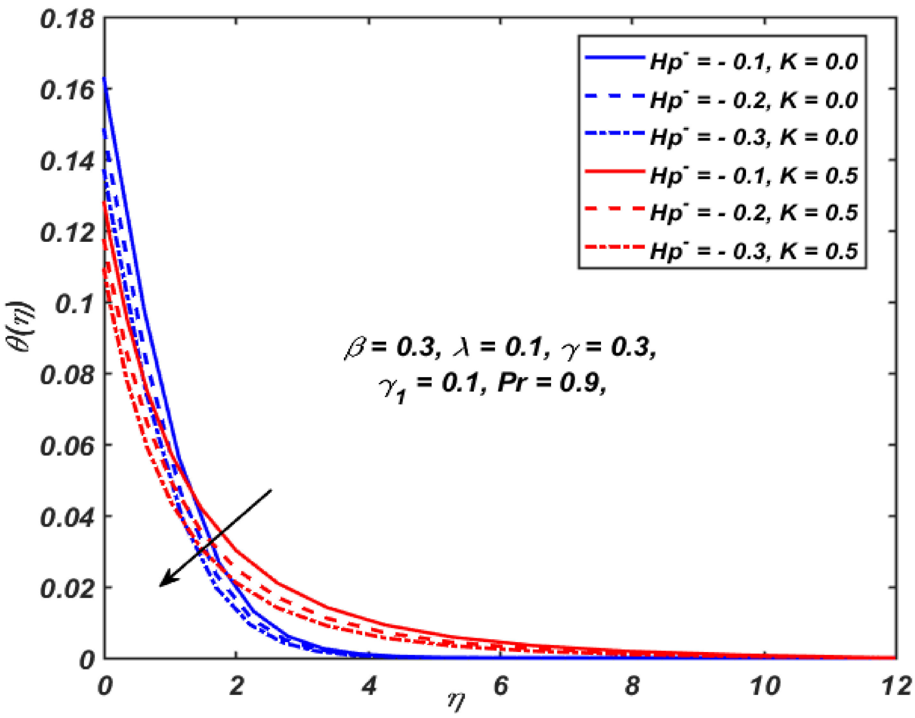

Figure 10. Impact of Hp^- on $\theta(\eta)$ for plate/cylinder.

Tables 1 and 2 analyze the impacts of emerging parameters on skin friction coefficient for plate and cylindrical surfaces, respectively. Particularly, Table 1 reports the skin friction coefficient variations at the flat surface for different values of mixed convection parameter λ and Casson fluid parameter β, and the magnetic field parameter γ. We noticed that the skin friction coefficient tends to decrease (in an absolute sense) for positive values of the Casson fluid parameter and the mixed convection parameter. Furthermore, the outcomes are in contrast for a magnetic field parameter γ that is for higher values of magnetic field parameter the skin friction coefficient enhances. Table 2 shows the impact of the Casson fluid parameter, mixed convection, and magnetic field parameter on the skin friction coefficient at the cylindrical surface. We observed that for both the positive Casson fluid parameter and mixed convection parameter, the skin friction coefficient declines, whereas the opposite is the case for magnetic field parameter. From both Tables 1 and 2, we have seen that the magnitude for cylindrical surface is enlarged as compared with flat plate.

The influences of the Prandtl number, heat generation and heat absorption parameters, and the Newtonian heating parameter on heat transfer rate on both flat plate and cylindrical surfaces are presented in Tables 3 and 4, respectively, with a fixed Casson fluid parameter $\beta = 0.3$, mixed convection parameter $\lambda = 0.1$, and magnetic field parameter $\gamma = 0.3$. From Tables 3 and 4, we seen that the heat transfer rate for both the plate and cylinder increases significantly (in an absolute sense) for higher values of Hp^+ and Newtonian heating parameter γ_1, whereas Pr and Hp^- have a reducing impact on the heat transfer rate. Table 5 presents comparative values of Nusselt number with the existing literature. We found an excellent match that validates the present results.

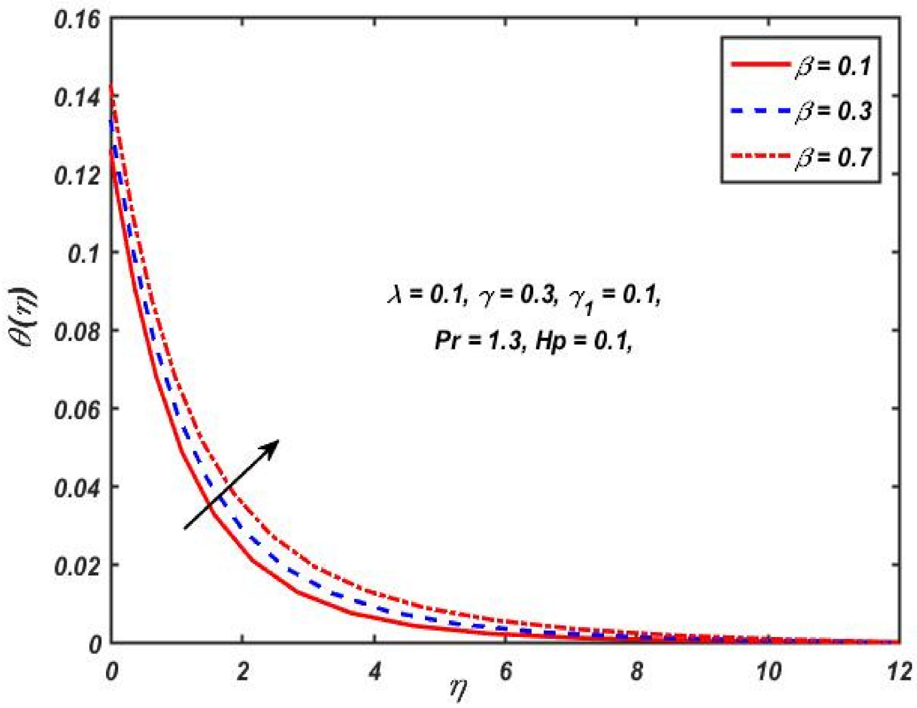

Figure 11. Impact of β on $\theta(\eta)$.

Table 1. Variation in skin friction for the plate.

β	λ	γ	**Skin Friction Coefficient**
0.1	0.1	0.3	−3.4705
0.2	0.1	0.3	−2.5500
0.25	0.1	0.3	−2.3260
0.3	1.0	0.3	−2.0772
0.3	3.0	0.3	−1.8909
0.3	5.0	0.3	−1.7115
0.3	0.1	0.1	−2.0833
0.3	0.1	0.5	−2.3177
0.3	0.1	0.9	−2.79001

Table 2. Variation in skin friction for the cylinder.

β	λ	γ	**Skin Friction Coefficient**
0.1	0.1	0.3	−5.8949
0.2	0.1	0.3	−3.7782
0.25	0.1	0.3	−3.3305
0.3	1.0	0.3	−2.9356
0.3	3.0	0.3	−2.7484
0.3	5.0	0.3	−2.5703
0.3	0.1	0.1	−2.9403
0.3	0.1	0.5	−3.1821
0.3	0.1	0.9	−3.6765

Table 3. Variation in Nusselt number for the plate.

Pr	Hp^{+}	Hp^{-}	γ_1	$-\theta'(0)$
1.2	0.1	0.1	0.1	−0.1170
1.4	0.1	0.1	0.1	−0.1153
1.6	0.1	0.1	0.1	−0.1140
1.2	0.1	0.1	0.1	−0.1170
1.2	0.2	0.1	0.1	−0.1199
1.2	0.3	0.1	0.1	−0.1247
1.2	0.1	−0.1	0.1	−0.1163
1.2	0.1	−0.2	0.1	−0.1124
1.2	0.1	−0.3	0.1	−0.1115
1.2	0.1	0.1	0.10	−0.1170
1.2	0.1	0.1	0.13	−0.1603
1.2	0.1	0.1	0.15	−0.1918

Table 4. Variation in Nusselt number for the cylinder.

Pr	Hp^{+}	Hp^{-}	γ_1	$-\theta'(0)$
1.2	0.1	0.1	0.1	−0.1140
1.4	0.1	0.1	0.1	−0.1128
1.6	0.1	0.1	0.1	−0.1119
1.2	0.1	0.1	0.1	−0.1140
1.2	0.2	0.1	0.1	−0.1170
1.2	0.3	0.1	0.1	−0.1236
1.2	0.1	−0.1	0.1	−0.1111
1.2	0.1	−0.2	0.1	−0.1102
1.2	0.1	−0.3	0.1	−0.1095
1.2	0.1	0.1	0.10	−0.1140
1.2	0.1	0.1	0.13	−0.1547
1.2	0.1	0.1	0.15	−0.1839

Table 5. Nusselt number comparison with existing results.

Pr	Present Outcomes	Mukhopadhyay [32]	Bidin and Nazar [33]
1.0	0.9544	0.9547	0.9547
3.0	1.4702	1.4714	1.4714
3.0	1.8952	1.8961	1.8961

5. Conclusions

Non-Newtonian fluid passed through stretching surfaces has been investigated numerically. The comparative impacts of flow variables on velocity and temperature profiles are analyzed for both flat plate and cylindrical surfaces. We observed that Casson fluid velocity results in a declining nature towards the magnetic field parameter because of enhancements in the Lorentz force. Such results hold for both flat plate and cylindrical surfaces. The temperature of fluid exerts a direct relationship towards Newtonian heating, magnetic field, and heat generation parameters, whereas the opposite is the case for the Prandtl number and heat absorption parameters. The variation magnitude for the cylindrical surface is significant as compared with a flat plate. The skin friction coefficient leads to a decrease for the cylinder as well as a flat plate with an increase in Casson fluid and mixed convection parameters. The local Nusselt number decreases for large values of Prandtl number, whereas it increases for the Newtonian heating parameter. Collectively, the effects of parameters on fluid flow over the cylinder are more prominent than the plate.

Author Contributions: Conceptualization, methodology, formal analysis; writing—original draft preparation, K.U.R.; visualization, validation, data curation, supervision, W.S.; Investigation, project administration, validation, data curation, S.A.; Investigation, Writing—review and editing, supervision.; N.K. All authors have read and agreed to the published version of the manuscript.

Funding: This research received no external funding.

Institutional Review Board Statement: Not applicable.

Informed Consent Statement: Not applicable.

Data Availability Statement: All data is available in manuscript.

Acknowledgments: The authors would like to thank Prince Sultan University, Saudi Arabia, for the technical support through the TAS research lab.

Conflicts of Interest: The authors declare no conflict of interest.

Nomenclature

$\overline{\mathbf{V}}$	Velocity field
ρ	Fluid density
p	Fluid pressure
$D/D\bar{t}$	Material time derivative
$\bar{u}, \bar{v}$	Velocity components (dimensional)
$\bar{x}, \bar{r}$	Cylindrical coordinates (dimensional)
υ	Kinematic viscosity
B_0	Magnetic field constant
β	Casson fluid parameter
σ	Fluid electrical conductivity
g	Gravitational acceleration
$\beta^*{}_T$	Thermal expansion coefficient
$\overline{T}$	Fluid temperature (dimensional)
$\overline{T}_\infty$	Ambient temperature
K_1	Thermal conductivity
c_p	Specific heat capacity at constant pressure

Q_0	Heat generation/absorption coefficient
U_0	Reference velocity
$\overline{R}$	Radius of cylinder
$\overline{\psi}$	Stream function
L	Characteristic length
$\theta(\eta)$	Fluid temperature (dimensionless)
$f\prime(\eta)$	Fluid velocity (dimensionless)
K	Curvature parameter
λ	Mixed convection parameter
γ	Magnetic field parameter
Pr	Prandtl number
Hp^+	Heat generation parameter
Hp^-	Heat absorption parameter
γ_1	Newtonian heating parameter
Gr	Grashof number
h_s	Heat transfer coefficient
τ_w	Shear stress
μ	Dynamic viscosity
q_w	Heat flux at surface
Abbreviations	
PDEs	Partial differential equations
ODEs	Ordinary differential equations
MHD	Magnetohydrodynamics
HAM	Homotopy analysis method

References

1. Crane, L.J. Flow past a stretching plate. *Z. Angew. Math. Phys. ZAMP* **1970**, *21*, 645–647. [CrossRef]
2. Gupta, P.S.; Gupta, A.S. Heat and mass transfer on a stretching sheet with suction or blowing. *Can. J. Chem. Eng.* **1977**, *55*, 744–746. [CrossRef]
3. Dutta, B.; Roy, P.; Gupta, A. Temperature field in flow over a stretching sheet with uniform heat flux. *Int. Commun. Heat Mass Transf.* **1985**, *12*, 89–94. [CrossRef]
4. Char, M.I. Heat transfer of a continuous, stretching surface with suction or blowing. *J. Math. Anal. Appl.* **1988**, *135*, 568–580.
5. Vajravelu, K. Viscous flow over a nonlinearly stretching sheet. *Appl. Math. Comput.* **2001**, *124*, 281–288. [CrossRef]
6. Sajid, M.; Hayat, T. Influence of thermal radiation on the boundary layer flow due to an exponentially stretching sheet. *Int. Commun. Heat Mass Transf.* **2008**, *35*, 347–356. [CrossRef]
7. Khan, W.A.; Pop, I. Boundary-layer flow of a nanofluid past a stretching sheet. *Int. J. Heat Mass Transf.* **2010**, *53*, 2477–2483. [CrossRef]
8. Malik, M.Y.; Hussain, A.; Salahuddin, T.; Awais, M.; Bilal, S.; Khan, F. Flow of Sisko fluid over a stretching cylinder and heat transfer with viscous dissipation and variable thermal conductivity: A numerical study. *AIP Adv.* **2016**, *6*, 045118. [CrossRef]
9. Rehman, K.U.; Khan, A.A.; Malik, M.; Zehra, I.; Ali, U. Temperature and concentration stratification effects on non-Newtonian fluid flow past a cylindrical surface. *Results Phys.* **2017**, *7*, 3659–3667. [CrossRef]
10. Siddiqa, S.; Begum, N.; Ouazzi, A.; Hossain, M.A.; Gorla, R.S. Heat transfer analysis of Casson dusty flu-id flow along a vertical wavy cone with radiating surface. *Int. J. Heat Mass Transf.* **2018**, *127*, 589–596. [CrossRef]
11. Souayeh, B.; Machireddy, G.R.; Sreenivasulu, P.; Poornima, T.; Rahimi-Gorji, M.; Alarifi, I.M. Comparative analysis on non-linear radiative heat transfer on MHD Casson nanofluid past a thin needle. *J. Mol. Liq.* **2019**, *284*, 163–174. [CrossRef]
12. Prajapati, Y.K. Influence of fin height on heat transfer and fluid flow characteristics of rectangular microchannel heat sink. *Int. J. Heat Mass Transf.* **2019**, *137*, 1041–1052. [CrossRef]
13. Hamid, M.; Usman, M.; Khan, Z.; Haq, R.; Wang, W. Heat transfer and flow analysis of Casson fluid enclosed in a partially heated trapezoidal cavity. *Int. Commun. Heat Mass Transf.* **2019**, *108*, 104284. [CrossRef]
14. Sheikh, N.A.; Ching, D.L.C.; Khan, I.; Kumar, D.; Nisar, K.S. A new model of fractional Casson fluid based on generalized Fick's and Fourier's laws together with heat and mass transfer. *Alex. Eng. J.* **2019**, *59*, 2865–2876. [CrossRef]
15. Nandeppanavar, M.M.; Vaishali, S.; Kemparaju, M.C.; Raveendra, N. Theoretical analysis of thermal characteristics of casson nano fluid flow past an exponential stretching sheet in Darcy porous media. *Case Stud. Therm. Eng.* **2020**, *21*, 100717. [CrossRef]
16. Zhang, L.; Tian, L.; Zhang, A.; Chen, H. Effects of the shape of tube and flow field on fluid flow and heat transfer. *Int. Commun. Heat Mass Transf.* **2020**, *117*, 104782. [CrossRef]
17. Khan, Z.H.; Khan, W.A.; Hamid, M.; Liu, H. Finite element analysis of hybrid nanofluid flow and heat transfer in a split lid-driven square cavity with Y-shaped obstacle. *Phys. Fluids* **2020**, *32*, 093609. [CrossRef]

18. Yang, W.; Chen, X.; Jiang, Z.; Zhang, X.; Zheng, L. Effect of slip boundary condition on flow and heat transfer of a double fractional Maxwell fluid. *Chin. J. Phys.* **2020**, *68*, 214–223. [CrossRef]
19. Wilk, J. Heat/mass transfer analogy in the case of convective fluid flow through minichannels. *Int. J. Therm. Sci.* **2020**, *156*, 106467. [CrossRef]
20. Abdelmalek, Z.; Khan, I.; Khan, M.W.; Rehman, K.U.; Sherif, E.S. Computational analysis of nano-fluid due to a non-linear variable thicked stretching sheet subjected to Joule heating and thermal radiation. *J. Mater. Res. Technol.* **2020**, *9*, 11035–11044. [CrossRef]
21. Rafiq, T.; Mustafa, M.; Farooq, M.A. Modeling heat transfer in fluid flow near a decelerating rotating disk with variable fluid properties. *Int. Commun. Heat Mass Transf.* **2020**, *116*, 104673. [CrossRef]
22. Rehman, K.U.; Shatanawi, W.; Abodayeh, K. Thermophysical aspects of magnetized Williamson fluid flow subject to both porous and non-porous surfaces: A Lie symmetry analysis. *Case Stud. Therm. Eng.* **2021**, *28*, 101688. [CrossRef]
23. Javaherdeh, K.; Karimi, H.; Azarbarzin, T. Lattice Boltzmann simulation of fluid flow and heat transfer in a micro channel with heat sources located on the walls. *Superlattices Microstruct.* **2021**, *160*, 107069. [CrossRef]
24. Rehman, K.U.; Shatanawi, W.; Shatnawi, T.A. On Thermal Energy Transport Complications in Chemically Reactive Liquidized Flow Fields Manifested with Thermal Slip Arrangements. *Energies* **2021**, *24*, 8530. [CrossRef]
25. Ahmad, S.; Khan, M.N.; Nadeem, S.; Rehman, A.; Ahmad, H.; Ali, R. Impact of Joule heating and multiple slips on a Maxwell nanofluid flow past a slendering surface. *Commun. Theor. Phys.* **2021**, *74*, 015001. [CrossRef]
26. Rehman, K.U.; Shatanawi, W.; Zahri, M.; Sherif, E.-S.M.; Junaedi, H.; Lv, Y.-P. Thermal analysis on uniformly heated diamond obstruction in convective liquid suspension. *Case Stud. Therm. Eng.* **2021**, *26*, 101062. [CrossRef]
27. Usman, M.; Zubair, T.; Hamid, M.; Haq, R.U.; Khan, Z.H. Unsteady flow and heat transfer of tangent-hyperbolic fluid: Legendre wavelet-based analysis. *Heat Transf.* **2020**, *50*, 3079–3093. [CrossRef]
28. Wang, F.; Rehman, S.; Bouslimi, J.; Khaliq, H.; Qureshi, M.I.; Kamran, M.; Alharbi, A.N.; Ahmad, H.; Farooq, A. Comparative study of heat and mass transfer of generalized MHD Oldroyd-B bio-nano fluid in a permeable medium with ramped conditions. *Sci. Rep.* **2021**, *11*, 23454. [CrossRef] [PubMed]
29. Rehman, K.U.; Shatanawi, W.; Abodayeh, K. A group theoretic analysis on heat transfer in MHD thermally slip Carreau fluid subject to multiple flow regimes (MFRs). *Case Stud. Therm. Eng.* **2022**, *30*, 101787. [CrossRef]
30. Zubair, T.; Usman, M.; Nisar, K.S.; Hamid, M.; Mahmoud, E.E.; Yahia, I. Investigation of shape effects of Cu-nanoparticle on heat transfer of MHD rotating flow over nonlinear stretching sheet. *Alex. Eng. J.* **2021**, *61*, 4457–4466. [CrossRef]
31. Tamoor, M.; Waqas, M.; Khan, M.I.; Alsaedi, A.; Hayat, T. Magnetohydrodynamic flow of Casson fluid over a stretching cylinder. *Results Phys.* **2017**, *7*, 498–502. [CrossRef]
32. Mukhopadhyay, S. MHD boundary layer flow and heat transfer over an exponentially stretching sheet embedded in a thermally stratified medium. *Alex. Eng. J.* **2013**, *52*, 259–265. [CrossRef]
33. Bidin, B.; Nazar, R. Numerical solution of the boundary layer flow over an exponentially stretching sheet with thermal radiation. *Eur. J. Sci. Res.* **2009**, *33*, 710–717.